Biosensors and Bioelectronics 142 (2019) 111517

Contents lists available at ScienceDirect

Biosensors and Bioelectronics

journal homepage: www.elsevier.com/locate/bios

Ultrasensitive electrochemiluminescence immunosensor for the detection of amyloid-β proteins based on resonance energy transfer between g-C_3N_4 and Pd NPs coated NH_2-MIL-53

Jinglong Fang, Guanhui Zhao, Xue Dong, Xuan Li, Juncong Miao, Qin Wei, Wei Cao*

Key Laboratory of Interfacial Reaction & Sensing Analysis in Universities of Shandong, School of Chemistry and Chemical Engineering, University of Jinan, Jinan, 250022, PR China

ARTICLE INFO

Keywords:
Electrochemiluminescence
Resonance energy transfer
Au NPs functionalized graphitic carbon nitride
Pd NPs doped metal organic framework

ABSTRACT

An electrochemiluminescence (ECL) analytical platform was proposed for ultrasensitive detection of amyloid-β proteins (Aβ) based on the ECL resonance energy transfer (ECL-RET). In this work, gold nanoparticles-functionalized graphitic carbon nitride nanosheets (g-C_3N_4@Au NPs) and palladium nanoparticles-coated Metal organic framework (Pd NPs@NH_2-MIL-53) were synthesized, which were as ECL donor and ECL acceptor respectively. A strong cathode ECL emission was obtained from the g-C_3N_4@Au NPs when used $K_2S_2O_8$ as its co-reactant. Here, Au NPs not only was used as an accelerator to enhance and stabilize the ECL signal, but also a connector for attaching Aβ antibody. In addition, NH_2-MIL-53(Al) was selected as a label material for supporting Pd NPs to synergistically increase the intensity and range of UV-visible absorption. The ECL signal of g-C_3N_4@Au NPs was intensely decreased when the ECL acceptor probe Pd NPs@NH_2-MIL-53 was incubated onto the modified GCE by way of the specific recognition. Under the optimal condition, a wide detection range from 10 fg/mL to 50 ng/mL and a low detection limit of 3.4 fg/mL (S/N = 3) were obtained. In consideration of favorable specificity, stability and reproducibility, the proposed method was successfully applied for Aβ detection in actual human serum samples and could be a potential analytical tool for sensitive molecular trace detection in clinical analysis.

1. Introduction

Alzheimer's disease (AD), as a latent and chronic neurodegenerative disorders, has caused entire world health problem and huge emotional panic. AD is original characterized by learning and memory impairment loss and eventually result memory decline and cognitive dysfunction with no effective disease-improvement therapy available at present (Thapa et al., 2016). Amyloid-β proteins (Aβ), as a polypeptide containing 39-43 amino acids, is considered to be the cause of neuronal death and is widely recognized as a biomarker of AD (Shankar et al., 2007). In fact, Aβ is deposited early in the disease process decades before symptoms occur. Therefore, accurate detection of Aβ is very critical for the timely diagnosis and treatment of diseases (Wang et al., 2018). $Aβ_{1-42}$ and $Aβ_{1-40}$ are the two major forms of Aβ proteins, $Aβ_{1-42}$ is more hydrophobic than $Aβ_{1-40}$ and is more likely to aggregate (Vestergaard et al., 2005). In this work, $Aβ_{1-42}$ was used as a protein model to prepare immunosensor. In the past few years, hard work has been done on the quantify detection of Aβ, such as Fluorescence Resonance Energy Transfer, Surface Plasmon Resonance Biosensor, electrochemical immunosensor, photoelectrochemical immunosensor and so on (Hegnerová et al., 2009; Jiang et al., 2018; Liu et al., 2013; Wang et al., 2018). Currently, the application of electrochemiluminescence (ECL) technology in Aβ detection (Ke et al., 2018) has attracted much attention due to its simplicity and sensitivity.

Electrochemiluminescence (ECL) become a widely used analytical technique involving many fields such as biological analysis (Shao et al., 2018), environment monitoring (Shi et al., 2017) and pharmaceutical analysis (Wei et al., 2016; Yang et al., 2011) because of its high sensitivity, simple operation, good controllability in time and space, and low background (Li et al., 2016). As one of many mechanisms to enhance or quench the ECL response, ECL resonance energy transfer (ECL-RET) has been shown to be an effective signaling mechanism for the development of the highly sensitive and specific ECL biosensing system. A key aspect of ECL-RET has been reported was that the proper spectral overlap between the donor's ECL spectrum and the acceptor's absorption spectrum (Huo et al., 2018). Researchers have been working to

* Corresponding author.
E-mail addresses: jncw88@163.com, jn_chm302@163.com (W. Cao).

https://doi.org/10.1016/j.bios.2019.111517
Received 7 May 2019; Received in revised form 27 June 2019; Accepted 14 July 2019
Available online 16 July 2019
0956-5663/

initiate appropriate matching ECL-RET donor-receptor pairs and to establish various ECL-RET sensing platforms for analysis of different substances such as ions (Babamiri et al., 2018), protein (Sha et al., 2019) and RNA (Huo et al., 2018).

As a metal-free polymeric semiconductor, graphitic carbon nitride (g-C_3N_4) has gained increasing research concerns with unique and versatile properties. G-C_3N_4 as a fascinating ECL emitter, amazed the researchers in virtue of their high quantum yields, high stable chemical properties and nontoxicity (Fu et al., 2019; Jin et al., 2018). In addition, g-C_3N_4 is easy to manipulate in functionalization or element doping, so many materials such as polymers, biomolecules, metals or metal oxide nanoparticles have been used for synergistic integration with g-C_3N_4 to improve the performance of g-C_3N_4 and expand its range of applications (Liang et al., 2018). Gold Nanoparticles (Au NPs) have been widely studied and shown significant potential in biological and medical applications owing to their unique physicochemical properties such as large specific surface area (Saha et al., 2012) and good electrical conductivity (Annamalai et al., 2013). Au NPs are often used as carrier materials and luminescent catalysts in the ECL field (Al-Hinaai et al., 2018). And ECL-RET between Au NPs and luminescent reagents can also be used to construct enhanced or quenched ECL biosensors (Cao et al., 2018; Zhang et al., 2018; Zhao et al., 2018). Therefore, g-C_3N_4@Au NPs as a platform enhanced the sensitivity and stability of immunosensors by stabilizing electron transfer and effectively immobilizing Aβ antibody.

The metal-organic framework (MOF) consists of organic ligand and metal ion, which has many excellent properties such as large surface area and permanent pores, and was easy to change the pores and surface function according to the demand (Hou et al., 2018). In the field of sensing, their flexible and porous structure facilitates the diffusion of guest molecules into an infinitely and highly ordered frame, thereby promoting host-guest interactions (Zhou et al., 2018). Thus, the MOF may be a well carrier material (Yang et al., 2018). NH_2-MIL-53(Al) with flexible frameworks exhibits good chemical stability in water (Boule et al., 2018). In addition, the presence of amino groups in the surface of NH_2-MIL-53(Al) generally endows the good interaction between MOF particles and various polymers. More important, the ultraviolet light absorption of NH_2-MIL-53(Al) can be applied to build annihilation sensors under the action of enhancer. As a member of precious metal nanoparticles, palladium nanoparticles (Pd NPs) are of wide interest due to their large surface areas (Suresh Kumar et al., 2015) and specific catalytic (Wang et al., 2013). Simultaneously, Pd NPs has a wide range of UV absorption available (Wang et al., 2012) and is capable of enhancing the absorption at specific locations through the combination with other substances. Therefore, Pd NPs@NH_2-MIL-53(Al) which as a quencher of the proposed sensor was labeled onto Aβ antibody.

In this work, an ultrasensitive quenching ECL immunosensor based on ECL-RET between g-C_3N_4@Au NPs and Pd NPs@NH_2-MIL-53 was constructed for the trace of Aβ. The as-prepared g-C_3N_4@Au NPs nanocomposites expressed stronger and more stable cathodic ECL emission compared with individual g-C_3N_4 nanomaterial, and a notable ECL signal diminishing effect was observed in the performance of the biosensor when Pd NPs@NH_2-MIL-53 nanocomposites were incubated onto the immunosensor. In addition, the constructed sensor also received favorable analytical feedback for the determination of Aβ in actual human serum samples and exhibited an accurate and reliable detection platform for clinical diagnosis of this assay.

2. Experience sections

2.1. Reagents and apparatuses

The surface morphology of the sample was obtained from scanning electron microscopy (SEM, Zeiss, Germany) and Transmission electron microscopic (TEM, JEOL1400, Japan). X-ray diffraction (XRD) patterns were obtained using D8 focus diffractometer (Bruker AXS, Germany). Fourier transform infrared spectroscopy (FT-IR) spectrogram was recorded by VERTEX70 Spectrometer (Bruker Co. Germany). Electrochemical measurements were recorded with a CHI760D workstation (Shanghai Chenhua Instruments, China). The ECL signal was detected with a MPI-E Electrochemiluminescence Analyzer (Xi'an Remax Analyse Instrument Co. Ltd). A common three-electrode system was employed during the experiment with a modified glassy carbon electrode (GCE, 4.0 mm in diameter) as working electrode, a platinum wire as the auxiliary electrode and Ag/AgCl (saturated KCl solution) as reference electrode.

N-hydroxysulfosuccinimide (NHS), carbodiimide hydrochloride (EDC) and 2-amino-benzene-1,4-dicarboxylic acid (5.3 mmol,H_2BDC-NH_2) were obtained from Aladdin Reagent Database Inc. (Shanghai, China). Bovine serum albumin (BSA) was purchased from Sigma-Aldrich (Beijing, China). Aβ antigen (Aβ, Subtypes $Aβ_{1-42}$) and Aβ antibody (Ab_1, Ab_2) were gained from Biocell Science Co. Ltd (Shanghai, China). Urea, Sodium tetrachloropalladate (Na_2PdCl_4), Chloroauric acid ($HAuCl_4$) and N,N-Dimethylformamide (DMF) was obtained from Shanghai Chemical Reagent Co. Ltd. Aluminum nitrate nonahydrate ($Al(NO)_3{\cdot}9H_2O$), Sodium borohydride ($NaBH_4$) and sodium hydroxide (NaOH) were obtained from Sinopharm Chemical Reagent Co. Ltd (Shanghai, China). The phosphate buffer solutions (PBS) with various pH values were prepared by mixing Na_2HPO_4 and KH_2PO_4, and adjusted by 0.1 M NaOH. Ultrapure water was used for the experiments. All other reagents used in this research were analytical pure and used without further purification.

2.2. Synthesis process of g-C_3N_4@Au NPs composites

The g-C_3N_4@Au NPs contact system was prepared according to previous literature with tiny changes (Chen et al., 2014). Briefly, 100 mg of the as-prepared bulk g-C_3N_4 was added into 20 mL ultra-pure water under ultrasonic irradiation for 30 min. Then 1 mL 2% $HAuCl_4$ solution was dissolved in the g-C_3N_4 dispersion and stirred for 30 min at the room temperature. Soon afterwards, 5 mg of PVP was added into the solution in order to prevent the aggregation of Au nanoparticles. After that, the freshly 20 μL prepared $NaBH_4$ solution (0.3 g/mL) was slowly added into the above solution with continuous stirring for 60 min. Finally, to obtain the g-C_3N_4@Au NPs composite, the mixture was centrifuged at 8000 rpm for several times and dried in an oven at 60 °C and the powder was saved at 4 °C.

2.3. Synthesis process of Pd NPs@NH_2-MIL-53@Ab_2

The approach of preparing Pd NPs@NH_2-MIL-53 has been improved by In-suit reduction. 50 mg of NH_2-MIL-53 was dispersed into 10 mL of ultrapure water and following added 2 mL of 2% Na_2PdCl_4 solution stirring for 15 min. Hereafter, 5 mg of PVP was added into the solution to prevent the agglomeration of Pd nanoparticles. Then 5 mL of 5 mol/L sodium citrate solution and a drop of $NaBH_4$ solution were added to the prepared solution and stirred for 8 h to reduce Na_2PdCl_4 to Pd nanoparticles. Finally, the generated Pd NPs@NH_2-MIL-53 nanoparticles were centrifuged at 8000 rpm for 10 min and rinsed with deionized water for four times. The desirable solid was dried under vacuum at 60 °C overnight. 5 mg Pd NPs@NH_2-MIL-53, 500 μL EDC (10 mmol) and NHS (5 mmol) mixture PBS (pH 7.4) solution, 250 μL Ab_2 (10 μg/mL) and 1 mL PBS (pH 7.4) were incubated at 4 °C for 24 h, then the mixture was centrifuged at 11000 rpm for 5 min and dissolved in 1 mL PBS for further use.

2.4. Construction of the biosensor

Scheme 1 shows the schematic diagram of the quenching ECL immunosensor. Originally, the GCE was polished by 0.3 and 0.05 μm alumina powder and cleaned by ultra-pure water and dried in air. 8 μL of g-C_3N_4@Au NPs solution was coated onto electrodes and dried in

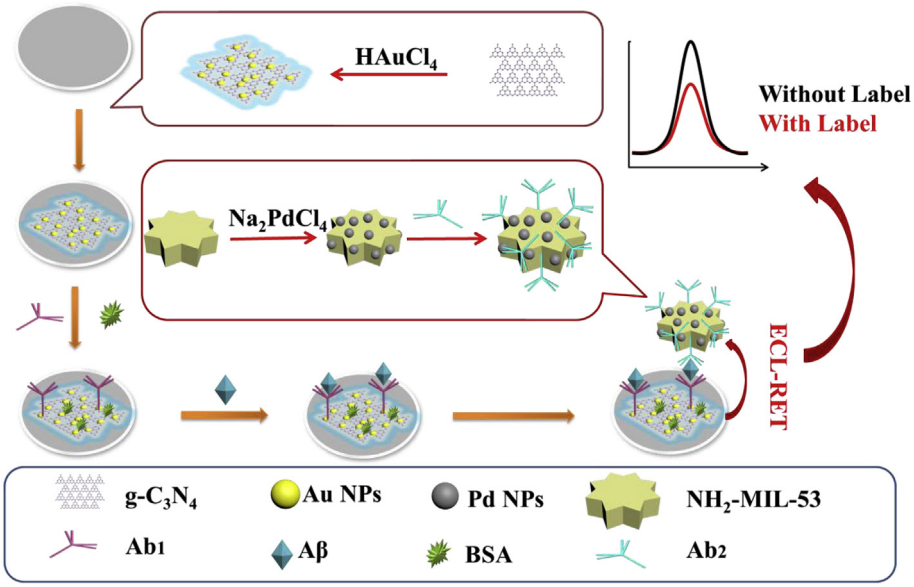

Scheme 1. The schematic illustration of the electrochemiluminescence immunosensor.

room temperature, then putting 6 μL Ab_1 on g-C_3N_4@Au NPs-modified GCE. Afterwards, 3 μL BSA (1%) was covered on GCE with 45 min for blocking non-specific binding site when the GCE was dried in 4 °C. After careful washing with PBS, surface-modified GCE was ligated with 6 μL of various amounts of Aβ for 45 min at 4 °C. After that, 6 μL Pd NPs@NH_2-MIL-53@Ab_2 solutions were added to the modified GCE to incubate for 45 min at 4 °C and rinsed by PBS. The constructed ECL immunosensor was stored at 4 °C for the following testing.

3. Results and discussion

3.1. Characterization of materials

As shown in Fig. 1A, it can be seen clearly in the TEM image that the prepared g-C_3N_4 is lamellar structure. Meanwhile, it could be found from SEM image (Fig. 1B) that small bright spots with a size of 15 ± 2 nm were distributed uniformly on the g-C_3N_4 after the g-C_3N_4 is functionalized by Au NPs, and EDS spectrum of g-C_3N_4@Au NPs externalized in Fig. S1 confirmed that the nanocomposites contain C, N and Au elements, demonstrating the successful preparation of g-C_3N_4@Au NPs. Moreover, XRD pattern of NH_2-MIL-53 was displayed in Fig. 1C, all the peaks were in accordance with standard simulated XRD spectrum peaks (The Cambridge Crystallographic Data Centre, access structures 847257). As Fig. S2 delivered, the SEM morphology of NH_2-MIL-53 was uniformly three-dimensional star structure assembled by diamond cubes with an average diameter of 500 nm, which show exactly the successful preparation of NH_2-MIL-53. Because H_2BDC-NH_2 served as an organic ligand to synthesize NH_2-MIL-53, the surface of NH_2-MIL-53 has numerous amino groups which could link with Ab_2. As shown in the FT-IR spectrogram (Fig. S3), the absorption peak at 3496 and 3386 cm^{-1} was the stretching vibration of N–H, proving the presence of amino groups. The SEM image of the prepared Pd NPs@NH_2-MIL-53 (Fig. 1D) not only maintained uniformly three-dimensional star structure assembled by diamond cubes but revealed that small bright spots with a size of 20 ± 2 nm grown on its exterior. And the EDS spectrum as shown in Fig. S4 further demonstrated the Pd NPs was attached on NH_2-MIL-53.

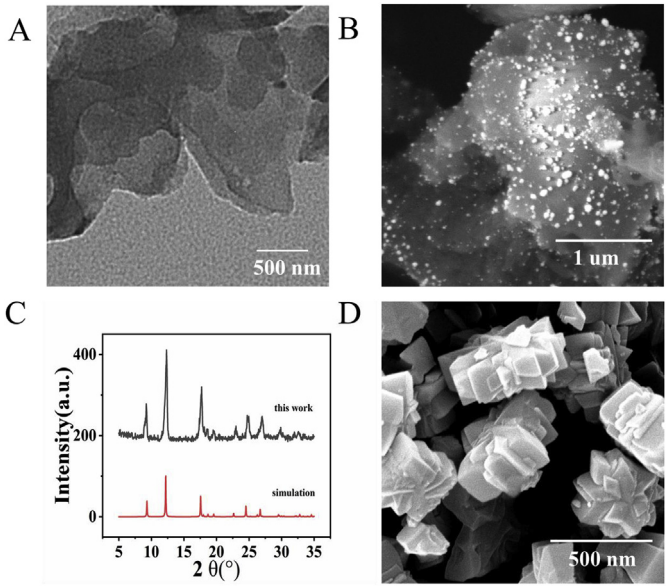

Fig. 1. (A) TEM image of g-C_3N_4, (B) SEM image of g-C_3N_4@Au NPs, (C) XRD pattern of NH_2-MIL-53, (D) SEM image of Pd NPs@NH_2-MIL-53.

3.2. Detection mechanism of the ECL biosensor

The g-C_3N_4 which was assembled with Au NPs displayed cathode emission light in the existence of co-reactant $K_2S_2O_8$ at the voltage range from -1.2 - 0 V. Discussion of the g-C_3N_4 - $K_2S_2O_8$ system ECL mechanism was based on relevant reference reports (Li et al., 2014). The route showed ECL mechanism to generate excited-state g-C_3N_4*: g-C_3N_4 was reduced directly on the electrode and primarily $S_2O_8^{2-}$ was reduced to $SO_4^{\bullet-}$ and then g-$C_3N_4^{\bullet-}$ reacted with $SO_4^{\bullet-}$ to generate g-C_3N_4*. A stronger ECL signal is released over the transition from the excited state to the ground state.

$$g\text{-}C_3N_4 + e^- \rightarrow g\text{-}C_3N_4^{\bullet-} \quad (1)$$

$$S_2O_8^{2-} + e^- \rightarrow SO_4^{2-} + SO_4^{\bullet-} \quad (2)$$

$$g\text{-}C_3N_4^{\bullet-} + SO_4^{\bullet-} \rightarrow g\text{-}C_3N_4^{*} + g\text{-}C_3N_4 \quad (3)$$

$$g\text{-}C_3N_4^{*} \rightarrow g\text{-}C_3N_4 + h\nu \quad (4)$$

The ECL behaviors of the g-C_3N_4 modified GCE and g-C_3N_4@Au NPs modified GCE were detected in PBS (pH 7.4) containing 80 mM $K_2S_2O_8$ to verify the catalytic property of Au NPs. As shown in Fig. 2A, the ECL

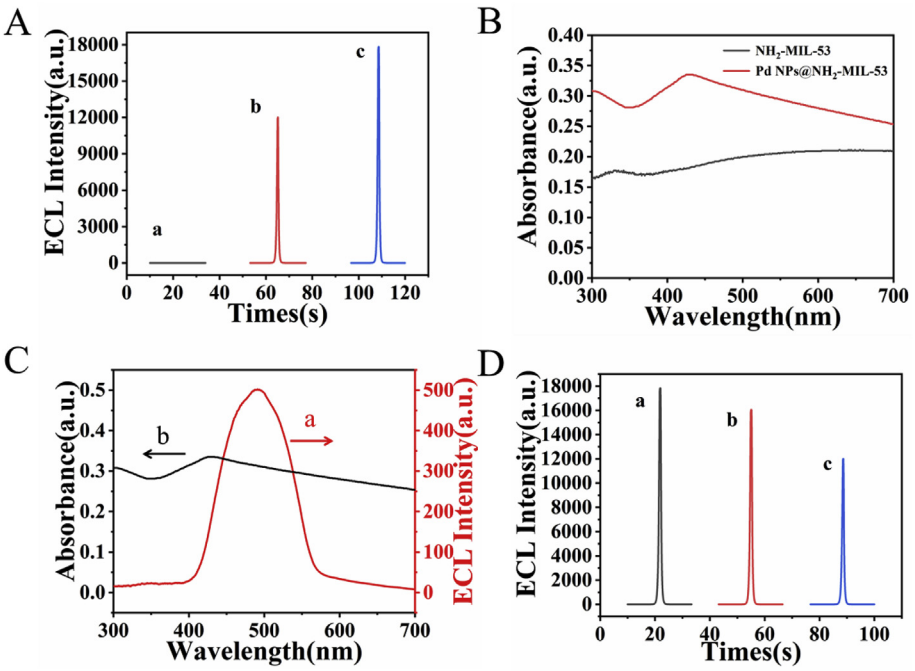

Fig. 2. (A) ECL behavior of bare GCE (a), g-C_3N_4 nanosheets (b), g-C_3N_4@Au NPs composite (c), (B) UV–vis absorption spectra of NH_2-MIL-53 (curve black) and Pd NPs@NH_2-MIL-53 (curve red), (C) UV–vis absorption spectra of Pd NPs@NH_2-MIL-53 (cover b) and ECL emission spectrum of g-C_3N_4 (cover a) and (D) ECL behavior of g-C_3N_4@Au NPs/GCE (a), NH_2-MIL-53/g-C_3N_4@Au NPs/GCE (b), Pd NPs@NH_2-MIL-53/g-C_3N_4@Au NPs/GCE (c). (For interpretation of the references to colour in this figure legend, the reader is referred to the Web version of this article.)

signal from curve b to curve c increased with the Au NPs catalytic effect. Hybridization of g-C_3N_4 with Au NPs may lead to over-injection of g-C_3N_4 conduction band (CB) by partial transfer of electrons to Au NPs, thereby preventing g-C_3N_4 from being electrochemically degraded and simultaneously catalyzing persulfate reduction of ($S_2O_8^{2-}$) to pore donor ($SO_4^{\bullet-}$) resulting in enhanced ECL emission of g-C_3N_4 (Chen et al., 2014). As depicted in Fig. 2B, the UV-Vis absorption spectra exhibited enhancement from NH_2-MIL-53 (curve black) to Pd NPs@NH_2-MIL-53 (curve red) respectively. It could be observed from Fig. 2C that the Pd NPs@NH_2-MIL-53 can quench the ECL emission of g-C_3N_4 due to the large overlap between the ECL emission spectrum of g-C_3N_4 (cover a) and the UV-Vis absorption spectrum of Pd NPs@NH_2-MIL-53 (cover b). What can be discovered from Fig. 2D that NH_2-MIL-53 weakened the ECL signal due to electron transfer obstruction and resonance energy transfer effect, and significant quenching effect was showed between Au NPs functionalized g-C_3N_4 and Pd NPs@NH_2-MIL-53. On the basis of the ECL-RET mechanism, a new ECL sensor was proposed to sensitively detect Aβ.

3.3. Electrochemical and Electrochemiluminescence behaviors of the biosensor

Electrochemical and Electrochemiluminescence behaviors are significant method to support the progressive manufacturing of the immunosensor. Performed in PBS (pH = 7.4) containing 0.1 M $K_2S_2O_8$ and 0.1 M KCl, Fig. 3A shows the ECL-potential curves of the electrode under different modified states. A strong ECL signal was produced on the g-C_3N_4@Au/GCE electrode. When the composite of Pd NPs@ NH_2-MIL-53@Ab_2 was modified on the surface of Aβ/Ab_1/g-C_3N_4@Au NPs/GCE, the ECL signals decreased greatly, it can be explained that ECL-RET occurring between Pd NPs@NH_2-MIL-53 and g-C_3N_4@Au NPs effectively reduced ECL emission.

Electrochemical impedance spectroscopy (EIS) was also carried to characterize the fabrication of the sensor. The Nyquist plots of EIS (Fig. 3B) in the electrode fabrication process was recorded in 2.5 mM $[Fe(CN)_6]^{4-}$/$[Fe(CN)_6]^{3-}$ containing 0.1 M KCl. Compared with the bare GCE (curve a), an obviously increased electron transfer resistance (Ret, the semicircle diameter in the impedance spectrum) was discovered at the g-C_3N_4@Au NPs/GCE modified GCE (curve b), ascribing to the poor conductivity of g-C_3N_4@Au NPs/GCE, Comparing with g-C_3N_4@Au NPs/GCE (curve b), the resistance (curve c, d and e) becomes larger gradually due to the nonconductive materials (Ab_1, BSA and Aβ) impeding the electron transfer when they were linked to the g-C_3N_4@Au NPs/GCE modified GCE. The resistance values significantly increased after the electrode was successively connected with Pd NPs@NH_2-MIL-53@Ab_2. The above experimental results confirmed that the immunosensor was constructed successfully.

3.4. Optimization analysis

To optimize the performance of the modified sensor in the analysis of Aβ, the concentration of $K_2S_2O_8$, g-C_3N_4@Au NPs, Pd NPs@NH_2-MIL-53 and the influence of pH were evaluated. Fig. 4A shows the relationship between the concentration of $K_2S_2O_8$ and the resulting ECL signal. It could be observed that the ECL signal increased as the concentration of $K_2S_2O_8$ was enhanced in the lower concentration region while decreased when the concentration of $K_2S_2O_8$ is larger than 80 mmol/L. Thus, 80 mmol/L was selected as the optimal $K_2S_2O_8$ concentration.

G-C_3N_4 illustrated extraordinary ECL capability, while too much of it would trigger self-absorption behavior which would shrink the ECL response and then affect the sensitivity and stability of the immunosensor. As shown in Fig. 4B, the ECL signal increased when the concentration of g-C_3N_4@Au NPs was less than 2 mg/mL while decreased when the concentration was greater than 2 mg/mL. Therefore, 2 mg/mL g-C_3N_4@Au NPs was used in the ECL system. Because Pd NPs@NH_2-MIL-53 was the energy recipient in the ECL-RET system, the amount of Pd NPs@NH_2-MIL-53 could interfere the degree of energy transmission. What can be observed from Fig. 4C that the ECL signal tended to poor decrease after 2 mg/mL. Hence, 2 mg/mL of Pd NPs@ NH_2-MIL-53 was chosen as the optimal concentration.

Moreover, the pH of PBS would disturb the ECL luminescence intensity. It could be observed from Fig. 4D that the response signal increased rapidly on lowering the pH from 5.3 to 7.4 and decreased also rapidly after 7.4, because high or low pH can adversely affect the immobilization process of proteins. Thus, near-neutral pH 7.4 is selected as the optimal pH.

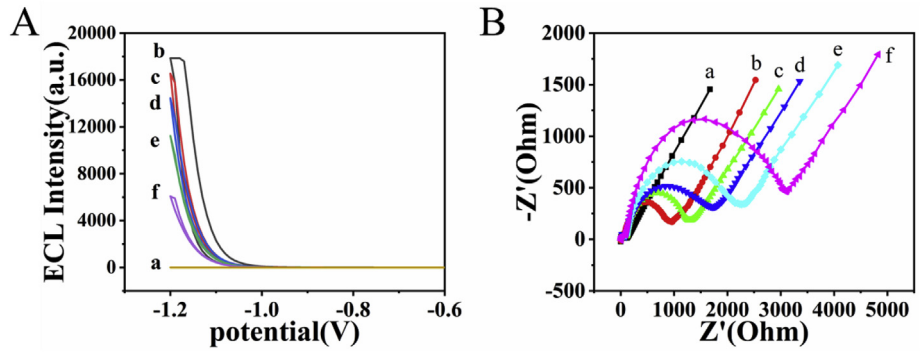

Fig. 3. ECL–potential curves (A) and the Nyquist plots of EIS (B) of the electrode under different modified states: GCE (a), g-C_3N_4@Au NPs/GCE (b), Ab_1/g-C_3N_4@Au NPs/GCE (c), BSA/Ab_1/g-C_3N_4@Au NPs/GCE (d), Aβ/BSA/Ab_1/g-C_3N_4@Au NPs/GCE (e), Pd NPs@NH_2-MIL-53@Ab_2/Aβ/BSA/Ab_1/g-C_3N_4@Au NPs/GCE (f).

3.5. Detection of Aβ via the ECL biosensor

To analyze the capability of the immunosensor, different concentrations of Aβ were detected underneath optimal conditions. In this work, Fig. 5A exhibited the tendency in ECL intensity by testing a catena of Aβ with concentrations from 0.01 pg/mL to 50 ng/mL. The calibration curve (Fig. 5B) was displayed by drafting the ECL intensity against the logarithm of Aβ concentration with the equation was I_{ECL} = 4543.98325–670.76919 × log c (R^2 = 0.995). Has been calculated, ultralow detection limit was 3.4 fg/mL (S/N = 3), which is much lower than that of other detection methods (Table S1). The above experimental results demonstrated that the immunosensor with high sensitivity based on site-fixed antibody immobilization can achieve Aβ detection at the femtogram level.

3.6. Stability, selectivity and repeatability of sensors

Stability, selectivity and repeatability are three of the most considerable indicators worth testing when judging the function of the immunosensor. Multiple detection results were shown in Fig. S5 to confirm the truth of these three properties. The stability of the ECL biosensor was examined by consecutive cyclic potential scans for 14 cycles. As depicted in Fig. S5, the ECL intensity showed no obvious addition or decline. The results demonstrated the excellent storage stability of the proposed biosensor. The Selectivity of the designed biosensor was further investigated. Compared against other four possible interferences, including prostate-specific antigen (PSA), carcinoembryonic antigen (CEA), α-fetoprotein (AFP), Human Serum Albumin (HAS), the ECL response toward the targets of Aβ and the mixture has significant decline with RSD was less than 5%, indicating that the immunosensor demonstrated eminent selectivity for the detection of Aβ. Moreover, in order to investigate the repeatability, a series of modified electrodes were prepared for the detection of 0.01 ng/mL of Aβ and stored at 4 °C when not in use. Results were showed in Fig. S5 that RSDs were 1.1%, suggesting that the fabricated immunosensor performed a good reproducibility and precision.

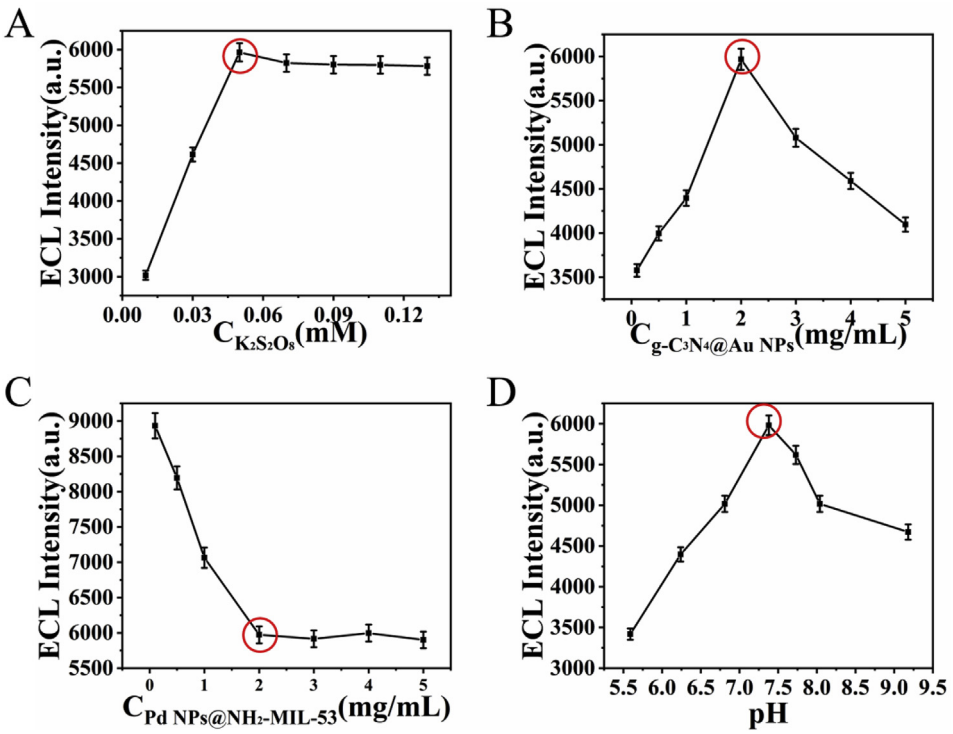

Fig. 4. The optimization of experimental conditions of $K_2S_2O_8$ concentration (A), g-C_3N_4@Au NPs concentration (B), Pd NPs@NH_2-MIL-53 concentration (C) and pH (D), error bar = RSD (n = 5), Aβ = 0.01ng/mL.

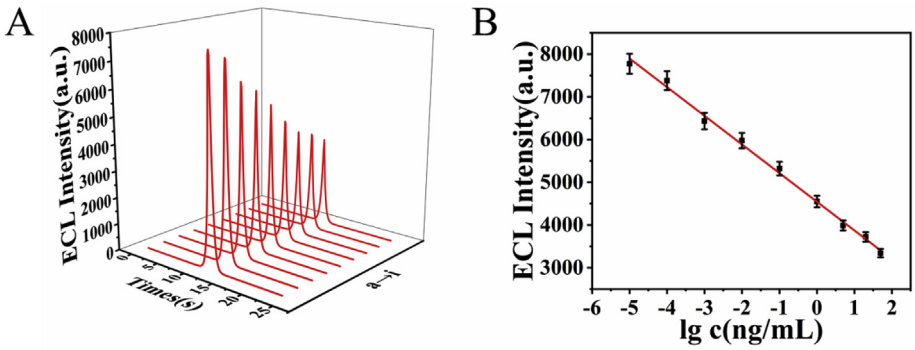

Fig. 5. (A,B) ECL response of the immunosensor for the detection of different concentrations of Aβ: (a) 0.01 pg/mL, (b) 0.1 pg/mL, (c) 1 pg/mL, (d) 10 pg/mL, (e) 100 pg/mL, (f) 1 ng/mL, (g) 5 ng/mL, (h) 20 ng/mL, (i) 50 ng/mL, error bar = RSD (n = 5).

3.7. Analysis of actual samples

In order to verify the clinical application of the proposed immunosensor, the concentration of Aβ in the human serum was determined and the accurateness with the standard addition method was verified. The outcome was illustrated in Table S2. The relative standard deviation (RSD) was less than 5% and the recovery was within the range of 95–105%, which illustrated the favorable potential possibility of clinical application.

4. Conclusion

In summary, a quenching ECL immunosensor in view of ECL-RET between Pd NPs@ NH_2-MIL-53 and g-C_3N_4-$S_2O_8^{2-}$ system was developed for the detection of Aβ. The prepared immunosensor exhibited excellent stability, accuracy and reproducibility with wide detection range from 10 fg/mL to 50 ng/mL and a low detection limit of 3.4 fg/mL (S/N = 3). Also, the immunosensor gave expression to favorable ECL response to Aβ Analysis of actual samples. Although the electrical conductivity defects of the MOF hinder its application, it is trusted that this sensing strategy could be applied to detect other biomarkers and establish potential tools for early diagnose of some diseases.

CRediT authorship contribution statement

Jinglong Fang: Data curation, Formal analysis, Writing - original draft. **Guanhui Zhao:** Formal analysis, Writing - review & editing. **Xue Dong:** Formal analysis. **Xuan Li:** Methodology, Formal analysis. **Juncong Miao:** Methodology, Formal analysis. **Qin Wei:** Funding acquisition, Project administration. **Wei Cao:** Writing - review & editing, Funding acquisition, Project administration.

Acknowledgments

This study was supported by the Natural Science Foundation of Shandong Province (No. ZR2016BM20), National Natural Science Foundation of China (No. 21575050, 21505051), National Key Scientific Instrument and Equipment Development Project of China (No. 21627809), Jinan Scientific Research Leader Workshop Project (2018GXRC024).

Appendix A. Supplementary data

Supplementary data to this article can be found online at https://doi.org/10.1016/j.bios.2019.111517.

References

Al-Hinaai, M.M., Kyaw, H.H., Al-Harthi, S.H., Khudaish, E.A., 2018. Sens. Actuators B Chem. 257, 460–468.
Annamalai, A., Christina, V.L., Sudha, D., Kalpana, M., Lakshmi, P.T., 2013. Colloids Surf B Biointerfaces 108, 60–65.
Babamiri, B., Salimi, A., Hallaj, R., 2018. Biosens. Bioelectron. 102, 328–335.
Boule, R., Roland, C., Le Polles, L., Audebrand, N., Ghoufi, A., 2018. Nanomaterials (Basel)pp. 8.
Cao, J.-T., Wang, Y.-L., Zhang, J.-J., Dong, Y.-X., Liu, F.-R., Ren, S.-W., Liu, Y.-M., 2018. Anal. Chem. 90, 10334–10339.
Chen, L., Zeng, X., Si, P., Chen, Y., Chi, Y., Kim, D.H., Chen, G., 2014. Anal. Chem. 86, 4188–4195.
Fu, X.L., Hou, F., Liu, F.R., Ren, S.W., Cao, J.T., Liu, Y.M., 2019. Biosens. Bioelectron. 129, 72–78.
Hegnerová, K., Bocková, M., Vaisocherová, H., Krištofiková, Z., Říčný, J., Řípová, D., Homola, J., 2009. Sens. Actuators B Chem. 139, 69–73.
Hou, Y., Liu, L., Zhang, Z., Sun, J., Zhang, Y., Jiang, J., 2018. Inorg. Chem. Commun. 95, 36–39.
Huo, X.L., Zhang, N., Yang, H., Xu, J.J., Chen, H.Y., 2018. Anal. Chem. 90, 13723–13728.
Jiang, M., Wang, X.-Y., Wang, X.-B., 2018. Chin. J. Anal. Chem. 46, 1339–1349.
Jin, Y., Kang, Q., Guo, X., Zhang, B., Shen, D., Zou, G., 2018. Anal. Chem. 90, 12930–12936.
Ke, H., Sha, H., Wang, Y., Guo, W., Zhang, X., Wang, Z., Huang, C., Jia, N., 2018. Biosens. Bioelectron. 100, 266–273.
Li, L., Chen, Y., Zhu, J.-J., 2016. Anal. Chem. 89, 358–371.
Li, X., Zhang, X., Ma, H., Wu, D., Zhang, Y., Du, B., Wei, Q., 2014. Biosens. Bioelectron. 55, 330–336.
Liang, R.P., Yu, L.D., Tong, Y.J., Wen, S.H., Cao, S.P., Qiu, J.D., 2018. Chem Commun (Camb) 54, 14001–14004.
Liu, L., Zhao, F., Ma, F., Zhang, L., Yang, S., Xia, N., 2013. Biosens. Bioelectron. 49, 231–235.
Saha, K., Agasti, S.S., Kim, C., Li, X., Rotello, V.M., 2012. Chem. Rev. 112, 2739–2779.
Sha, H., Zhang, Y., Wang, Y., Ke, H., Xiong, X., Jia, N., 2019. Biosens. Bioelectron. 124–125, 59–65.
Shankar, G.M., Bloodgood, B.L., Townsend, M., Walsh, D.M., Selkoe, D.J., Sabatini, B.L., 2007. J. Neurosci. 27, 2866–2875.
Shao, H., Lin, H., Lu, J., Hu, Y., Wang, S., Huang, Y., Guo, Z., 2018. Biosens. Bioelectron. 118, 247–252.
Shi, L., Li, X., Zhu, W., Wang, Y., Du, B., Cao, W., Wei, Q., Pang, X., 2017. ACS Sens. 2, 1774–1778.
Suresh Kumar, B., Amali, A.J., Pitchumani, K., 2015. ACS Appl. Mater. Interfaces 7, 22907–22917.
Thapa, A., Jett, S.D., Chi, E.Y., 2016. ACS Chem. Neurosci. 7, 56–68.
Vestergaard, M., Kerman, K., Saito, M., Nagatani, N., Takamura, Y., Tamiya, E., 2005. J. Am. Chem. Soc. 127, 11892–11893.
Wang, Y., Fan, D., Zhao, G., Feng, J., Wei, D., Zhang, N., Cao, W., Du, B., Wei, Q., 2018. Biosens. Bioelectron. 120, 1–7.
Wang, Z., Li, H., Zhen, S., He, N., 2012. Nanoscale 4, 3536–3542.
Wang, Z., Zheng, S., Cai, J., Wang, P., Feng, J., Yang, X., Zhang, L., Ji, M., Wu, F., He, N., Wan, N., 2013. Anal. Chem. 85, 11602–11609.
Wei, Y., Wang, H., Sun, S., Tang, L., Cao, Y., Deng, B., 2016. Biosens. Bioelectron. 86, 714–719.
Yang, H., Li, X.-c., Yang, F., Feng, J., Lin, M.-y., Chen, Z.-g., 2011. Microchimica Acta 175, 193–199.
Yang, X., Yu, Y.-Q., Peng, L.-Z., Lei, Y.-M., Chai, Y.-Q., Yuan, R., Zhuo, Y., 2018. Anal. Chem. 90, 3995–4002.
Zhang, A., Guo, W., Ke, H., Zhang, X., Zhang, H., Huang, C., Yang, D., Jia, N., Cui, D., 2018. Biosens. Bioelectron. 101, 219–226.
Zhao, G., Wang, Y., Li, X., Dong, X., Wang, H., Du, B., Cao, W., Wei, Q., 2018. ACS Appl. Mater. Interfaces 10, 22932–22938.
Zhou, Y., Yang, Q., Zhang, D., Gan, N., Li, Q., Cuan, J., 2018. Sens. Actuators B Chem. 262, 137–143.